Mathematical Modelling and Numerical Simulation with Applications, 2024, 4(5), 116–138

https://dergipark.org.tr/en/pub/mmnsa
ISSN Online: 2791-8564 / Open Access
https://doi.org/10.53391/mmnsa.1555392

RESEARCH PAPER

Boundary control of unsteady natural convective slip flow in reactive viscous fluids

Cansu Evcin [1,*,‡]

[1]Department of Mathematics, Faculty of Arts and Sciences, Tekirdağ Namık Kemal University, 59030 Tekirdağ, Türkiye

*Corresponding Author
‡cbilgir@nku.edu.tr (Cansu Evcin)

Abstract

We consider the optimal control of unsteady natural convective flow of reactive viscous fluid with heat transfer. It is assumed that Newton's law governs the heat transfer within an exothermic reaction under Arrhenius kinetics and Navier slip condition on the lower surface of the channel. The flow is examined in a vertical channel formed by two infinite vertical parallel plates, with a distance (H) between them. Time-dependent natural convective slip flow of reactive viscous fluid and heat transfer equations are solved in a unit interval using the Galerkin-Finite Element Method (FEM) with quadratic finite elements in space and the implicit Euler method in time. The direct solutions are obtained for testing various values of the problem parameters: the Biot number, the Frank Kamenetskii parameter, the Navier slip parameter, and the computation of the skin friction and the Nusselt number (Nu). The optimal control problem is designed for the momentum and energy equations to derive the fluid-prescribed velocity and temperature profiles by defining controls on the boundary of the domain in two ways: (a) controls are formulated as parameters in the boundary conditions, such as slip length and Biot number; (b) controls are assigned as time-dependent functions in the boundary conditions, representing the slip velocity and the heat transfer rate. Following a discretize-then-optimize approach to the control problem, optimization is performed by the SLSQP (Sequential Least Squares Programming) algorithm, a subroutine of SciPy. Numerically simulated results show that the proposed approach successfully drives the flow to prescribed velocity and temperature profiles.

Keywords: Convective slip flow; boundary control; FEM; Navier slip parameter; Biot number

AMS 2020 Classification: 65N30; 90C53; 93C20

1 Introduction

The problem of time-dependent free convective flow and heat transfer through vertical channels occurs widely in industrial applications such as solar heating and ventilating passive systems.

➤ **Received:** 25.09.2024 ➤ **Revised:** 20.12.2024 ➤ **Accepted:** 27.12.2024 ➤ **Published:** 31.12.2024

Additionally, some electronic devices with vertical circuit boards, including heat–generating elements, are designed with parallel heated plates. Moreover, the interaction between chemical reaction and natural convection arises within the fields of petrochemical industries and chemical engineering. Examples of such applications include chemical deposition systems, tubular laboratory reactors, the oxidation of solid materials in large containers, and many others. In this manner, several studies have been conducted by means of theoretical analysis and numerical simulations by researchers. Minto et al. [1] considered the free-convection flow in porous media driven by an exothermic catalytic chemical reaction represented by Arrhenius kinetics. They studied similarity and asymptotic solutions for temperature and concentration. Makinde [2] investigated the thermal stability of a reactive viscous fluid through a channel using perturbation technique together with a special type of Hermite-Pade approximation. Jha et al. studied the transient natural convection flow of reactive viscous fluid in a vertical channel [3] and in a tube [4] under Arrhenius kinetics, providing analytical and numerical approximations using perturbation and finite difference methods, respectively. Lately, the trapezoidal and Euler discretization methods have been used for the approximation of a numerical solution of augmented Urysohn-type nonlinear functional Volterra integral equations in [5, 6].

Although researchers in this topic traditionally consider no-slip condition for velocity, evidences for fluid slip have been reported for some microscale flows. For example, the effect of the slip boundary condition on the flow of fluids in a channel was studied by Rao and Rajagopal [7]. Then, Rundora and Makinde [8] investigated the effects of Navier slip on unsteady flow of a reactive variable viscosity non-Newtonian fluid. Additionally, Gbadeyan et al. [9] examined the effect of slip on natural convective flow and heat transfer of a viscous incompressible fluid using a domain decomposition method.

Results on the free convection flow with the slip condition attracted the attention of many researchers. Therefore, the analysis and control of chemically reactive and free convective flow have become one of the main subjects of optimal control problems. Tauviqirrahman et al. [10] applied a genetic algorithm to optimize the geometry of the complex slip surface by using location coordinates as design parameters. Another application of genetic algorithm was conducted by Zhang et al. [11] for optimizing the shape/pattern of boundary slip areas on bearing sliders. On the other hand, Hu and Wu [12] obtained the existence and uniqueness of optimal solutions for the active control of the flow velocity through the Navier slip boundary control. Moreover, an optimal control attempt was conducted by Haslinger and Mäkinen [13] to identify the slip bound function in the Stokes system with threshold slip boundary condition. Recently, Zhang and Zhu [14] developed an efficient Monte Carlo search for the optimal design of slip/no-slip configuration surfaces. Related literature and detailed theoretical results on the existence of optimal solutions corresponding to boundary control can be found in [15–18]. The majority of the studies focused on spatial control functions and, mostly, they have not been exemplified numerically. However, some physical and analytical approaches have been proposed by Joseph and Kamran [19], and Málek and Rajagopal [20].

The objective of the current work is to control the natural convective slip flow of reactive viscous fluid by using controls on the boundary of the domain. Motivated by previous results in the field [21–24] on the usage of parameters as control variables in fluid dynamics, we propose to maintain control of the fluid flow by using the parameters of the slip condition and Newtonian heating. 3. To the best of our knowledge, this is the first time that parameters such as slip length and Biot number are considered as controls to derive the velocity and heat transfer into desired states of the natural convective slip flow of reactive fluid in a PDE-constrained optimization framework. Moreover, reduction of the problem to one dimension in space enables the representation of the non-parametric parts of the boundary conditions as only time-dependent functions. This adds

another option to the type of control models, which is a function on the boundary depending only on time.

This paper is organized as follows. First, the physical formulation of the problem is introduced with the governing equations. Second, computational methods for the solution of PDEs in terms of space and time, and also for optimization, are presented. Third, numerical results and discussions on the direct FEM solutions and optimization algorithm are provided. Finally, the main contributions and findings of this study are summarized in the conclusion.

2 Problem statement

Physical formulation of the problem

We consider the optimal control of unsteady natural convective flow of reactive viscous fluid with heat transfer. It is assumed that the heat transfer follows Newton's law within an exothermic reaction under Arrhenius kinetics and the Navier slip condition on the lower surface of the channel. The flow is examined in a vertical channel formed by two infinite vertical parallel plates having a distance (H) between them, as shown in Figure 1. Following the work of Jha et al. [3], the dimensional governing equations are given as

$$\frac{\partial \bar{u}}{\partial \tau} = v\frac{\partial^2 \bar{u}}{\partial \bar{y}^2} + g\beta(\bar{\theta} - \bar{\theta}_0),$$
$$\frac{\partial \bar{\theta}}{\partial \tau} = \frac{k}{\rho C_p}\frac{\partial^2 \bar{\theta}}{\partial \bar{y}^2} + \frac{QC_0^* A}{\rho C_p} e^{(-\frac{E}{R\bar{\theta}})},$$

with the corresponding initial conditions

$$\bar{u} = 0, \quad \bar{\theta} \to \bar{\theta}_0 \quad \text{for} \quad 0 \le \bar{y} \le H, \quad \tau \le 0,$$

and boundary conditions for $\tau > 0$

$$\frac{\partial \bar{u}}{\partial \bar{y}} = \frac{\bar{u}}{\gamma^*}, \quad \frac{\partial \bar{\theta}}{\partial \bar{y}} = -\frac{h}{k}(\bar{\theta}_a - \bar{\theta}), \quad \text{at} \quad \bar{y} = 0,$$
$$\bar{u} = 0, \quad \bar{\theta} = \bar{\theta}_0 \quad \text{as} \quad \bar{y} \to H,$$

where $\bar{u}$ and $\bar{\theta}$ are the dimensional velocity and temperature of the fluid, respectively. Here, $\bar{\theta}_0$ is the initial fluid and wall temperature, β is the coefficient of thermal expansion, Q is the heat of reaction, A is the rate constant, E is the activation energy, R is the universal gas constant, v is the kinematic viscosity, C_0^* is the initial concentration of reactant species, g is the gravitational force, C_p is the specific heat at constant pressure, and k is the thermal conductivity of the fluid, ν is the kinematic viscosity and ρ is the density of the fluid.

The dimensionless form of the equations are derived by taking

$$y = \frac{\bar{y}}{H}, \quad t = \frac{\tau \mu_0}{H^2}, \quad \theta = \frac{E(\bar{\theta} - \bar{\theta}_0)}{R\bar{\theta}_0^2}, \quad u = \frac{\bar{u}\mu_0 E}{g\beta H^2 R\bar{\theta}_0^2}, \tag{1}$$

and

$$\epsilon = \frac{R\bar{\theta}_0}{E}, \quad \lambda = \frac{QC_0^* AEH^2}{R\bar{\theta}_0^2} e^{(-\frac{E}{R\bar{\theta}_0})}, \quad \text{Pr} = \frac{\mu_0 \rho C_p}{k}, \quad \gamma = \frac{\gamma^*}{H}, \; \theta_a = \frac{E(\bar{\theta}_a - \bar{\theta}_0)}{R\bar{\theta}_0^2}, \quad \text{Bi} = \frac{hH}{k}, \tag{2}$$

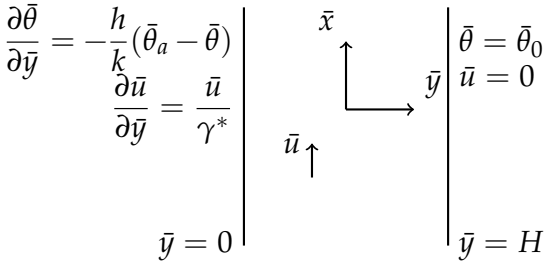

Figure 1. Physical configuration of the problem

where the definitions of the parameters are given as in the reference book [25]. Thus, the non-dimensional momentum and energy equations with dimensionless velocity u, temperature θ and time t are given as [26]

$$\frac{\partial u}{\partial t} = \frac{\partial^2 u}{\partial y^2} + \theta, \tag{3}$$

$$\frac{\partial \theta}{\partial t} = \frac{1}{\mathrm{Pr}}\frac{\partial^2 \theta}{\partial y^2} + \frac{\lambda}{\mathrm{Pr}} e^{\left(\frac{\theta}{1+\epsilon\theta}\right)}, \tag{4}$$

with the initial condition

$$u = 0,\ \theta = 0,\ 0 \le y \le 1,\ t = 0, \tag{5}$$

and boundary conditions when $t > 0$

$$\frac{\partial u}{\partial y} = \frac{u}{\gamma}, \qquad \frac{\partial \theta}{\partial y} = \mathrm{Bi}[\theta - \theta_a],\ \text{at}\ \Gamma_0, \tag{6}$$

$$u = 0, \qquad \theta = 0,\ \text{at}\ \Gamma_1, \tag{7}$$

where γ, Bi, Pr, λ, θ_a and ϵ are Navier slip parameter, Biot number, Prandtl number, Frank Kamenetskii parameter, ambient temperature and activation energy parameter and Γ_0 and Γ_1 denote the left ($y = 0$) and the right ($y = 1$) boundaries, respectively.

Boundary control approach

The optimal control problem is designed for the momentum and energy equations to derive the fluid-prescribed velocity and temperature profiles by defining controls on the boundary of the domain in two ways: (a) controls are assigned as time-dependent functions in the boundary conditions, representing the slip velocity and the heat transfer rate; (b) controls are formulated as the parameters in the boundary conditions, such as slip length (γ) and Biot number (Bi). Accordingly, the unsteady PDE-constrained optimal control problem comprising both cases is designed as follows:

$$\underset{f,g,\mathbf{c}}{\text{minimize}} \quad J((u,\theta);(f,g,\mathbf{c})) = \frac{\alpha_u}{2}\int_0^T\int_\Omega (u-u^d)^2 d\Omega dt + \frac{\alpha_\theta}{2}\int_0^T\int_\Omega (\theta-\theta^d)^2 d\Omega dt \tag{8}$$

$$+ \frac{\alpha_u}{2}\int_\Omega (u(T)-u^d(T))^2 d\Omega + \frac{\alpha_\theta}{2}\int_\Omega (\theta(T)-\theta^d(T))^2 d\Omega \tag{9}$$

$$+\frac{\alpha_f}{2}\int_0^T\int_\Omega f^2 d\Omega dt+\frac{\alpha_g}{2}\int_0^T\int_\Omega g^2 d\Omega dt+\frac{\alpha_c}{2}\int_\Omega \|\mathbf{c}\|^2 d\Omega, \tag{10}$$

subject to equations in (3)-(4). Here, $\alpha_u, \alpha_\theta, \alpha_f, \alpha_g$, and α_c are the regularization parameters and $u^d, \theta^d, u^d(T)$ and $\theta^d(T)$ are the desired velocity, desired temperature, desired velocity and desired temperature at final time T, respectively. Also, $\mathbf{c}$ is the vector of control parameters which denotes one or both of the parameters γ and Bi, $f(t)$ and $g(t)$ are time-dependent control functions in (6) at Γ_0 substituted as

$$f(t)=\frac{u(t,0)}{\gamma}, \quad \text{and} \quad g(t)=\mathrm{Bi}[\theta(t,0)-\theta_a(t,0)]. \tag{11}$$

In the sequel, controls are chosen as either from f and/or g functions or from the parameters γ and/or Bi.

3 Computational method

Time-dependent natural convective slip flow of reactive viscous fluid flow and heat transfer equations (3)-(4) are solved in a unit interval with the initial and boundary conditions in Eqs. (5)-(7) by using the finite element method in space and implicit Euler method in time.

Space discretization via finite element method

Setting the environment for a FEM solution requires the selection of the Sobolev spaces. For a general domain Ω, the inner product and the norm are defined as $\langle u,v\rangle_\Omega=\int_\Omega uv\,d\Omega$ and $\|v\|_{L^2(\Omega)}=\sqrt{\langle v,v,\rangle}$. Correspondingly,

$$H^1(\Omega)=\left\{v\ :\|v\|_{L^2(\Omega)}+\|\nabla v\|_{L^2(\Omega)}<\infty\right\},$$

$$H_0^1(\Omega)=\left\{v\in H^1(\Omega):v=0 \text{ on } \Gamma_1\right\}.$$

FEM solution is achieved through the derivation of the variational equations. Thus, (3)-(4) are multiplied by the test functions $(p,q)\in H_0^1(\Omega)^2$, respectively, for u and θ:

$$\int_\Omega\left(\frac{\partial u}{\partial t}-\frac{\partial^2 u}{\partial y^2}-\theta\right)p\,d\Omega=0,$$
$$\int_\Omega\left(\frac{\partial \theta}{\partial t}-\frac{1}{\mathrm{Pr}}\frac{\partial^2\theta}{\partial y^2}-\frac{\lambda}{\mathrm{Pr}}e^{\left(\frac{\theta}{1+\epsilon\theta}\right)}\right)q\,d\Omega=0.$$

Applying the Green's theorem and imposing the boundary conditions in (6), the variational formulation of the problem (3)-(4) yields: find $(u,\theta)\in H_0^1(\Omega)^2$ such that

$$\int_\Omega\frac{\partial u}{\partial t}p\,d\Omega+\int_\Omega\frac{\partial u}{\partial y}\frac{\partial p}{\partial y}\,d\Omega+\int_{\Gamma_0}\frac{u}{\gamma}\,p\,d\Gamma_0-\int_\Omega\theta p\,d\Omega=0,\quad p\in H_0^1(\Omega), \tag{12}$$

$$\int_\Omega\frac{\partial\theta}{\partial t}q\,d\Omega+\frac{1}{\mathrm{Pr}}\int_\Omega\frac{\partial\theta}{\partial y}\frac{\partial q}{\partial y}\,d\Omega+\frac{1}{\mathrm{Pr}}\int_{\Gamma_0}\mathrm{Bi}\,(\theta-\theta_a)\,q\,d\Gamma_0-\frac{\lambda}{\mathrm{Pr}}\int_\Omega e^{\left(\frac{\theta}{1+\epsilon\theta}\right)}q\,d\Omega=0,\quad q\in H_0^1(\Omega). \tag{13}$$

After that, finite dimensional approximations are introduced to employ quadratic finite elements. Let $\mathcal{T}_h$ be a division of Ω with size $h > 0$ and let $U_{h,0}$ and $Q_{h,0}$ be the space of quadratic polynomials on $\mathcal{T}_h$ and $U_{h,0},\ Q_{h,0} \subset H_0^1(\Omega)$. Now, the variational formulation is constructed for searching solutions such that $(u, \theta) \in U_{h,0} \times Q_{h,0}$. Properly, we define the basis functions $\{\xi_i\}_{i=1}^{\beta_u}$ and $\{v_k\}_{k=1}^{\beta_\theta}$ for $U_{h,0}$ and $Q_{h,0}$, respectively, as follows

$$u(t,y) \approx \sum_{j=1}^{\beta_u} u_j(t)\xi_j(y), \qquad \theta(t,y) \approx \sum_{l=1}^{\beta_\theta} \theta_l(t)v_l(y), \tag{14}$$

where $\mathbf{u} = (u_j(t))$ and $\boldsymbol{\theta} = (\theta_l(t))$ are the components of the vectors $\mathbf{u}$ and $\boldsymbol{\theta}$ at time t, respectively. So, the following approximations can be reached:

$$\frac{\partial u}{\partial t} \approx \sum_{j=1}^{\beta_u} \dot{u}_j(t)\xi_j(y), \qquad \frac{\partial \theta}{\partial t} \approx \sum_{l=1}^{\beta_\theta} \dot{\theta}_l(t)v_l(y), \tag{15}$$

$$\frac{\partial u}{\partial y} \approx \sum_{j=1}^{\beta_u} u_j(t)\frac{\partial \xi_j(y)}{\partial y}, \qquad \frac{\partial \theta}{\partial y} \approx \sum_{l=1}^{\beta_\theta} \theta_l(t)\frac{v_l(y)}{\partial y}, \tag{16}$$

$$e^{\frac{\theta}{1+\epsilon\theta}} \approx \sum_{l=1}^{\beta_\theta} e^{\frac{\theta_l}{1+\epsilon\theta_l}} v_l. \tag{17}$$

Here, $\dot{u}_j(t)$ and $\dot{\theta}_l(t)$ are the components of the discretized time derivatives. Substitution of the FEM approximations in Eqs. (14)-(17) into (12) and (13) results in the following:

$$\sum_{j=1}^{\beta_u} \dot{u}_j(t) \int_\Omega \xi_j\xi_i \, d\Omega + \sum_{j=1}^{\beta_u} u_j(t) \int_\Omega \frac{\partial \xi_j}{\partial y}\frac{\partial x_i}{\partial y} \, d\Omega - \sum_{l=1}^{\beta_\theta} \theta_l(t) \int_\Omega v_l\xi_i \, d\Omega + \frac{1}{\gamma}\sum_{j=1}^{\beta_u} u_j(t) \int_{\Gamma_0} \xi_j\xi_i \, d\Gamma_0 = 0,$$

$$\sum_{l=1}^{\beta_\theta} \dot{\theta}_l(t) \int_\Omega v_l v_k \, d\Omega + \frac{1}{\mathrm{Pr}}\sum_{l=1}^{\beta_\theta} \theta_l(t) \int_\Omega \frac{\partial v_l}{\partial y}\frac{\partial v_k}{\partial y} \, d\Omega - \frac{\lambda}{\mathrm{Pr}}\sum_{l=1}^{\beta_\theta} e^{\frac{\theta_l}{1+\epsilon\theta_l}} \int_\Omega v_l v_k \, d\Omega$$

$$+\frac{\mathrm{Bi}}{\mathrm{Pr}}\sum_{l=1}^{\beta_\theta} \theta_l(t) \int_{\Gamma_0} v_l v_k \, d\Gamma_0 - \frac{\mathrm{Bi}}{\mathrm{Pr}}\sum_{l=1}^{\beta_\theta} \theta_{a_l}(t) \int_{\Gamma_0} v_l v_k \, d\Gamma_0 = 0,$$

where $1 \le i \le \beta_u$ and $1 \le k \le \beta_\theta$. Accordingly, the coupled semi–discrete system of equations are formulated as

$$\begin{bmatrix} \mathbf{M} & \mathbf{0} \\ \mathbf{0} & \mathbf{S} \end{bmatrix} \begin{bmatrix} \dot{\mathbf{u}} \\ \dot{\boldsymbol{\theta}} \end{bmatrix} + \begin{bmatrix} \mathbf{K} + \frac{1}{\gamma}\mathbf{E} & -\mathbf{D} \\ \mathbf{0} & \mathbf{R} + \frac{\mathrm{Bi}}{\mathrm{Pr}}\mathbf{C} \end{bmatrix} \begin{bmatrix} \mathbf{u} \\ \boldsymbol{\theta} \end{bmatrix} + \begin{bmatrix} \mathbf{0} \\ \frac{\lambda}{\mathrm{Pr}}\mathbf{SN}(\boldsymbol{\theta}) \end{bmatrix} - \frac{\mathrm{Bi}}{\mathrm{Pr}} \begin{bmatrix} \mathbf{0} \\ \mathbf{C}\boldsymbol{\theta}_a \end{bmatrix} = \begin{bmatrix} \mathbf{0} \\ \mathbf{0} \end{bmatrix}, \tag{18}$$

where $\mathbf{M} = (M_{ij})$, $\mathbf{K} = (K_{ij})$, $\mathbf{D} = (D_{il})$, $\mathbf{E} = (E_{ij})$, $\mathbf{S} = (S_{kl})$, $\mathbf{R} = (R_{kl})$, $\mathbf{C} = (C_{kl})$ and

$$M_{ij} = \int_\Omega \xi_j \xi_i \, d\Omega, \qquad K_{ij} = \int_\Omega \frac{\partial \xi_j}{\partial y} \frac{\partial \xi_i}{\partial y} \, d\Omega, \qquad D_{il} = \int_\Omega v_l \xi_i \, d\Omega, \qquad E_{ij} = \int_{\Gamma_0} \xi_j \xi_i d\Gamma_0,$$
$$S_{kl} = \int_\Omega v_l v_k \, d\Omega, \qquad R_{kl} = \int_\Omega \frac{\partial v_l}{\partial y} \frac{\partial v_k}{\partial y} \, d\Omega, \qquad C_{kl} = \int_{\Gamma_0} v_l v_k d\Gamma_0.$$

To simplify, we define the following block matrices:

$$\mathbf{A}_1 = \begin{bmatrix} \mathbf{M} & \mathbf{0} \\ \mathbf{0} & \mathbf{S} \end{bmatrix}, \qquad \mathbf{A}_2 = \begin{bmatrix} \mathbf{K} + \frac{1}{\gamma}\mathbf{E} & -\mathbf{D} \\ \mathbf{0} & \mathbf{R} + \frac{\mathrm{Bi}}{\mathrm{Pr}}\mathbf{C} \end{bmatrix}, \qquad \mathbf{\Pi} = \begin{bmatrix} \mathbf{0}, \\ \frac{\lambda}{\mathrm{Pr}}\mathbf{SN}(\boldsymbol{\theta}) \end{bmatrix}, \qquad \mathbf{e} = \frac{\mathrm{Bi}}{\mathrm{Pr}} \begin{bmatrix} \mathbf{0} \\ \mathbf{C}\boldsymbol{\theta}_a \end{bmatrix}.$$

So, the semi-discrete problem can be given as

$$\mathbf{A}_1 \dot{\boldsymbol{\varphi}} + \mathbf{A}_2 \boldsymbol{\varphi} + \mathbf{\Pi}(\boldsymbol{\varphi}) = \mathbf{e} \qquad \text{for} \qquad \boldsymbol{\varphi} = (\mathbf{u}, \boldsymbol{\theta})^T. \tag{19}$$

Time discretization via implicit Euler method

The time derivative for $\boldsymbol{\varphi}$ is numerically approximated by the implicit Euler method using the following formula

$$\dot{\boldsymbol{\varphi}}^{n+1} \approx \frac{\boldsymbol{\varphi}^{n+1} - \boldsymbol{\varphi}^n}{\Delta t} \qquad \text{for} \qquad n = 0, 1, \ldots, N,$$

at $(n+1)$th time level. Thus, (19) can be rewritten as

$$\left(\frac{1}{\Delta t}\mathbf{A}_1 + \mathbf{A}_2 \right) \boldsymbol{\varphi}^{n+1} + \mathbf{\Pi}(\boldsymbol{\varphi}^{n+1}) - \frac{1}{\Delta t}\mathbf{A}_1 \boldsymbol{\varphi}^n - \mathbf{e} = 0 \quad \text{for} \quad n = 0, 1, \ldots, N, \tag{20}$$

which is a discrete non-linear system of equations in $\boldsymbol{\varphi}^{n+1}$. Here, $\boldsymbol{\varphi}^n$ and $\boldsymbol{\varphi}^{n+1}$ are obtained at the consecutive time levels t^n and t^{n+1} for $n = 1, \ldots, N$, iteratively, via Newton's method in the linearization. A closed form of (20) can be given as

$$\mathbf{F}_{n+1}(\boldsymbol{\varphi}^{n+1}) := L(\boldsymbol{\varphi}^{n+1})\boldsymbol{\varphi}^{n+1} + \mathbf{\Pi}(\boldsymbol{\varphi}^{n+1}) - \mathbf{d}^n = 0,$$

where L and $\mathbf{d}^n$ refer to the linear term and the known data from the previous time step, respectively and they are defined as

$$L = \frac{1}{\Delta t}\mathbf{A}_1 + \mathbf{A}_2, \qquad \mathbf{d}^n = \frac{1}{\Delta t}\mathbf{A}_1 \boldsymbol{\varphi}^n + \mathbf{e}.$$

As a result, fully discrete non-linear system of equations are formulated as

$$\mathbf{F}(\mathbf{\Phi}) = \begin{pmatrix} \mathbf{F}_1(\boldsymbol{\varphi}^1) \\ \mathbf{F}_2(\boldsymbol{\varphi}^2) \\ \vdots \\ \mathbf{F}_N(\boldsymbol{\varphi}^N) \end{pmatrix} = \begin{pmatrix} \mathbf{F}_1(\mathbf{u}^1, \boldsymbol{\theta}^1) \\ \mathbf{F}_2(\mathbf{u}^2, \boldsymbol{\theta}^2) \\ \vdots \\ \mathbf{F}_N(\mathbf{u}^N, \boldsymbol{\theta}^N) \end{pmatrix} = \mathbf{0}, \tag{21}$$

where $\mathbf{\Phi} = (\boldsymbol{\varphi}^1, \boldsymbol{\varphi}^2, \ldots, \boldsymbol{\varphi}^N)$.

Discretize–then–optimize approach

The approach to reach the optimal solution of the control problem depends on the discretized form. Therefore, the cost function in Eqs. (8)-(10) is reformulated using the discrete FEM approximations given in the previous section. The substitution of the discrete FEM solutions into $J((u,\theta);(f,g,\mathbf{c}))$ results in

$$\underset{\mathbf{f},\mathbf{g},\mathbf{c}}{\text{minimize}} \quad \mathbf{J}(\mathbf{\Phi};(\mathbf{f},\mathbf{g},\mathbf{c})) \tag{22}$$

$$\text{subject to} \quad \mathbf{F}(\mathbf{\Phi};(\mathbf{f},\mathbf{g},\mathbf{c})) = 0, \tag{23}$$

where $\mathbf{\Phi} = (\boldsymbol{\varphi}^1,\boldsymbol{\varphi}^2,\ldots,\boldsymbol{\varphi}^N)^T$, and $\mathbf{J}$ is the discrete objective function. In order to simplify, we denote all control variables $(\mathbf{f},\mathbf{g},\mathbf{c})$ by $\boldsymbol{m}$, then the discretized problem can be restated as follows:

$$\underset{\boldsymbol{m}}{\text{minimize}} \quad \mathbf{J}(\mathbf{\Phi};\boldsymbol{m}) \tag{24}$$

$$\text{subject to} \quad \mathbf{F}(\mathbf{\Phi};(\boldsymbol{m})) = 0. \tag{25}$$

Optimization step is initiated by construction of the Lagrangian function as

$$\mathcal{L}(\mathbf{\Phi},\boldsymbol{m},\mathbf{\Psi}) = \mathbf{J}(\mathbf{\Phi},\boldsymbol{m}) + \mathbf{\Psi}^*\mathbf{F}(\mathbf{\Phi},\boldsymbol{m}),$$

where $\mathbf{\Psi}$ denotes the Lagrange multiplier, the so-called adjoint variable. Accordingly, the first–order optimality conditions are established, considering the first order derivatives of the Lagrangian,

$$\nabla\mathcal{L}(\mathbf{\Phi},\boldsymbol{m},\mathbf{\Psi}) = \begin{pmatrix} \nabla\mathbf{J}(\mathbf{\Phi},\boldsymbol{m}) + \nabla\mathbf{F}(\mathbf{\Phi},\boldsymbol{m})^*\mathbf{\Psi} \\ \mathbf{F}(\mathbf{\Phi},\boldsymbol{m}) \end{pmatrix} = 0. \tag{26}$$

An optimal solution to problem in (24)–(25) has to be a root of (26). Therefore, Newton's method is employed as an iterative technique to find this root by calculating the Newton direction δ_k at iterate k

$$\nabla^2\mathcal{L}(\mathbf{\Phi}^k,\boldsymbol{m}^k,\mathbf{\Psi}^k)\delta^k = -\nabla\mathcal{L}(\mathbf{\Phi}^k,\boldsymbol{m}^k,\mathbf{\Psi}^k), \tag{27}$$

where $\delta^k = (\delta^k_\Phi,\delta^k_m,\delta^k_\Psi)$. Clearly, an open form of (27) leads to the system of equations as

$$\begin{bmatrix} \nabla^2_{(\Phi,m)}\mathcal{L}(\mathbf{\Phi}^k,\boldsymbol{m}^k,\mathbf{\Psi}^k) & \nabla_{(\Phi,m)}\mathbf{F}(\mathbf{\Phi}^k,\boldsymbol{m}^k)^* \\ \nabla_{(\Phi,m)}\mathbf{F}(\mathbf{\Phi}^k,\boldsymbol{m}^k) & \mathbf{0} \end{bmatrix} \begin{bmatrix} \begin{pmatrix} \delta^k_z \\ \delta^k_u \end{pmatrix} \\ \delta^k_\Psi \end{bmatrix} = - \begin{bmatrix} \nabla\mathbf{J}(\mathbf{\Phi}^k,\boldsymbol{m}^k) + \nabla_{(\Phi,m)}\mathbf{F}(\mathbf{\Phi}^k,\boldsymbol{m}^k)^*\mathbf{\Psi}^k \\ \mathbf{F}(\mathbf{\Phi}^k,\boldsymbol{m}^k) \end{bmatrix}. \tag{28}$$

Here, the updated formulas to iterate solutions are given as

$$\mathbf{\Phi}^{k+1} = \mathbf{\Phi}^k + \delta^k_z, \quad \boldsymbol{m}^{k+1} = \boldsymbol{m}^k + \delta^k_m, \quad \mathbf{\Psi}^{k+1} = \mathbf{\Psi}^k + \delta^k_\Psi.$$

This sequence of solutions can also be formulated as the first–order optimality conditions of the Sequential Quadratic Programming (SQP) subproblem defined as

$$\underset{s}{\text{minimize}} \quad \frac{1}{2}s^T\nabla^2_{(\Phi,m)}\mathcal{L}(\mathbf{\Phi}^k, \boldsymbol{m}^k, \mathbf{\Psi}^k)s + \nabla\mathbf{J}(\mathbf{\Phi}^k, \boldsymbol{m}^k, \mathbf{\Psi}^k)^*s \tag{29}$$

$$\text{subject to} \quad \nabla_{(\Phi,m)}\mathbf{F}(\mathbf{\Phi}^k, \boldsymbol{m}^k)^Ts + \mathbf{F}(\mathbf{\Phi}^k, \mathbf{m}^k) = 0, \tag{30}$$

where the solution vector s is the Newton direction in (28) corresponding to the update of $(\mathbf{\Phi}, \boldsymbol{m})$ variables. Additionally, the Lagrangian function related to the problem in (29)–(30) is established, called $\boldsymbol{\vartheta}$, with Lagrange multiplier μ as follows [27]:

$$\boldsymbol{\vartheta}(s,\mu) = \frac{1}{2}s^T\nabla^2_{(\Phi,m)}\boldsymbol{\mathcal{L}}(\mathbf{\Phi}^k, \boldsymbol{m}^k, \mathbf{\Psi}^k)s + \nabla\mathbf{J}(\mathbf{\Phi}^k, \boldsymbol{m}^k, \mathbf{\Psi}^k)^*s + \mu^*(\nabla_{(\Phi,m)}\mathbf{F}(\mathbf{\Phi}^k, \boldsymbol{m}^k)^Ts + \mathbf{F}(\mathbf{\Phi}^k, \mathbf{m}^k)).$$

Formally, the first–order optimality conditions of the SQP subproblem in (29)–(30) are given as

$$\begin{bmatrix} \nabla^2_{(\Phi,m)}\boldsymbol{\mathcal{L}}(\mathbf{\Phi}^k, \boldsymbol{m}^k, \mathbf{\Psi}^k) & \nabla_{(\Phi,m)}\mathbf{F}(\mathbf{\Phi}^k, \boldsymbol{m}^k)^* \\ \nabla_{(\Phi,m)}\mathbf{F}(\mathbf{\Phi}^k, \boldsymbol{m}^k) & \mathbf{0} \end{bmatrix} \begin{bmatrix} s \\ \mu \end{bmatrix} = - \begin{bmatrix} \nabla\mathbf{J}(\mathbf{\Phi}^k, \boldsymbol{m}^k) \\ \mathbf{F}(\mathbf{\Phi}^k, \boldsymbol{m}^k) \end{bmatrix}, \tag{31}$$

where $s = (\delta^k_\Phi, \delta^k_m)$ and $\mu = \mathbf{\Psi}^{k+1}$. A reformulation of the SQP subproblem is stated as

$$\underset{s}{\text{minimize}} \quad \frac{1}{2}s^T\mathbf{B}^ks + \nabla\mathbf{J}(\mathbf{\Phi}^k, \boldsymbol{m}^k, \mathbf{\Psi}^k)^Ts \tag{32}$$

$$\text{subject to} \quad \nabla_{(\Phi,m)}\mathbf{F}(\mathbf{\Phi}^k, \boldsymbol{m}^k)^Ts + \mathbf{F}(\mathbf{\Phi}^k, \mathbf{m}^k) = 0, \tag{33}$$

where we define $\mathbf{B}^k := \nabla^2_{(\Phi,m)}\boldsymbol{\mathcal{L}}(\mathbf{\Phi}^k, \boldsymbol{m}^k, \mathbf{\Psi}^k)$. This approach leads to the well-known SLSQP (Sequential Least Squares Programming) problem, as follows

$$\underset{s}{\text{minimize}} \quad \frac{1}{2}\|\mathbf{B}^ks + \nabla\mathbf{J}(\mathbf{\Phi}^k, \boldsymbol{m}^k)\|^2 \tag{34}$$

$$\text{subject to} \quad \nabla_{(\Phi,m)}\mathbf{F}(\mathbf{\Phi}^k, \boldsymbol{m}^k)^Ts + \mathbf{F}(\mathbf{\Phi}^k, \mathbf{m}^k) = 0. \tag{35}$$

Designed algorithms using SLSQP to deal with the problem in (34) by using a decomposition $\mathbf{B}^k = LDL^T$, and equivalently solves the following

$$\underset{s}{\text{minimize}} \quad \frac{1}{2}\|(D^k)^{1/2}(L^k)^Ts + (D^k)^{-1/2}(L^k)^{-1}\nabla\mathbf{J}(\mathbf{\Phi}^k, \boldsymbol{m}^k)\|^2 \tag{36}$$

$$\text{subject to} \quad \nabla_{(\Phi,m)}\mathbf{F}(\mathbf{\Phi}^k, \boldsymbol{m}^k)^Ts + \mathbf{F}(\mathbf{\Phi}^k, \mathbf{m}^k) = 0. \tag{37}$$

One can refer to [28–30] for details of the SLSQP algorithm and its usage in optimization. Also, a sketch of the underlying framework is presented to facilitate an easy follow-up in Algorithm 1.

Algorithm 1 Discretize–Then–Optimize Framework with SLSQP

1: Generate the fully discrete system of PDEs by FEM in space and Implicit Euler in time in (21).
2: Generate the discrete optimization problem in (22) and (23).
3: Initialize the optimization by an initial guess for the control.
4: Solve the SLSQP subproblem in (36) and (37) until $|\nabla\tilde{J}| < tol$ for a given tolerance.

4 Numerical results and discussions

FEM solution of the unsteady exothermic fluid flow and heat transfer equations

The unsteady exothermic fluid flow equations (3)-(4) with the boundary conditions (6)-(7) are solved using finite element method (FEM) in space and Implicit Euler scheme in time. The y-axis velocity profile and temperature distribution are obtained along the distance between parallel plates, $\Omega = [0, 1]$. Simulations are performed on a computer with Intel Core i7-10510 processor and 16GB RAM where Python programming language is used within the platform FEniCS [31] to solve PDEs. The non-linear system of equations is solved by the Newton's method at each simulation.

In this study, a quadratic finite element method is used on uniform mesh, consisting of 2^8 cells with 513 degrees of freedom for each subspace of the mixed finite element space. Discretization in time is executed by an Implicit Euler scheme with a uniform time step $\Delta t = 0.1$ Numerical results are obtained for various values of the Biot number, $0.1 \leq \text{Bi} \leq 1.5$, the Frank Kamenestskii parameter, $0.2 \leq \lambda \leq 0.8$, the Navier slip parameter, $0.1 \leq \gamma \leq 1.5$, the ambient temperature, $\theta_a = 1$ and the final time, $T = 0.4, 0.6, 0.8$. Mesh-dependent convergence tests are performed to validate the numerical results using the L^2 norm of the residuals between solutions obtained in consecutive mesh refinements. Figure 2a and Figure 2b depict the convergence in space and time, respectively. Specifically, these rates of convergence are shown together in Figure 2c at the same scale to highlight the difference in their sensitivity to refinements. That is, the convergence rates are inferred from the slopes of the lines in the space and time variables. Thus, as expected, the lines corresponding to the refinement in the time step, called as Time-Velocity and Time-Temperature, have slopes smaller than the lines corresponding to the refinement in space, called Space-Velocity and Space-Temperature. This is due to the employment of a first-order in time method, the Implicit Euler, and a quadratic finite element in space. In addition, Figure 2d depicts the CPU time costs for mesh refinements in time and space. It is observed that the refinement in time steps results in a larger cost than in space, but the choices used in the rest of this manuscript seem admissible.

Moreover, the method of discretization in time derivative is also investigated in terms of CPU time in Figure 3a and Figure 3b with the Crank-Nicolson method for the refinements in space and time variables, respectively. Since the number of function evaluations increases with the Crank-Nicolson method, the CPU costs are larger than those of the Implicit Euler method across all different meshes. Further, a mesh-dependent convergence comparison of Implicit Euler and Crank-Nicolson is also depicted in Figure 4a and Figure 4b. As the Implicit Euler is a first order and the Crank-Nicolson is a second-order method, the slopes of the lines clearly indicate these differences in both figures. In the end, the Implicit Euler is chosen to maintain the balance between costs and accuracy in approximations of solutions.

Figure 5a shows the velocity behavior for increasing values of λ and t. It can be seen that as λ and t increase the velocity magnitude increases. This tendency is also valid for the temperature as well in Figure 5b. Temperature rise occurs due to the strong chemical reaction and viscous heating sources in (4). This significant change in the temperature reduces the fluid viscosity and increases the velocity. Besides, due to the combined effects of the Navier slip condition, and asymmetric and convective heating of the plate, the temperature reaches the maximum value at the lower plate and decays to the upper plate of the channel.

Figure 6a and Figure 6b depict the variation of the velocity and temperature for increasing values of Biot number (Bi) and t. It is observed that the higher Bi higher the convective heating, velocity and temperature reach higher values at the lower plate. Also, an increase in Bi implies more convective heating at the lower plate which causes higher surface temperatures.

From Figure 7, one can deduce that increasing the Navier slip parameter γ increases the fluid

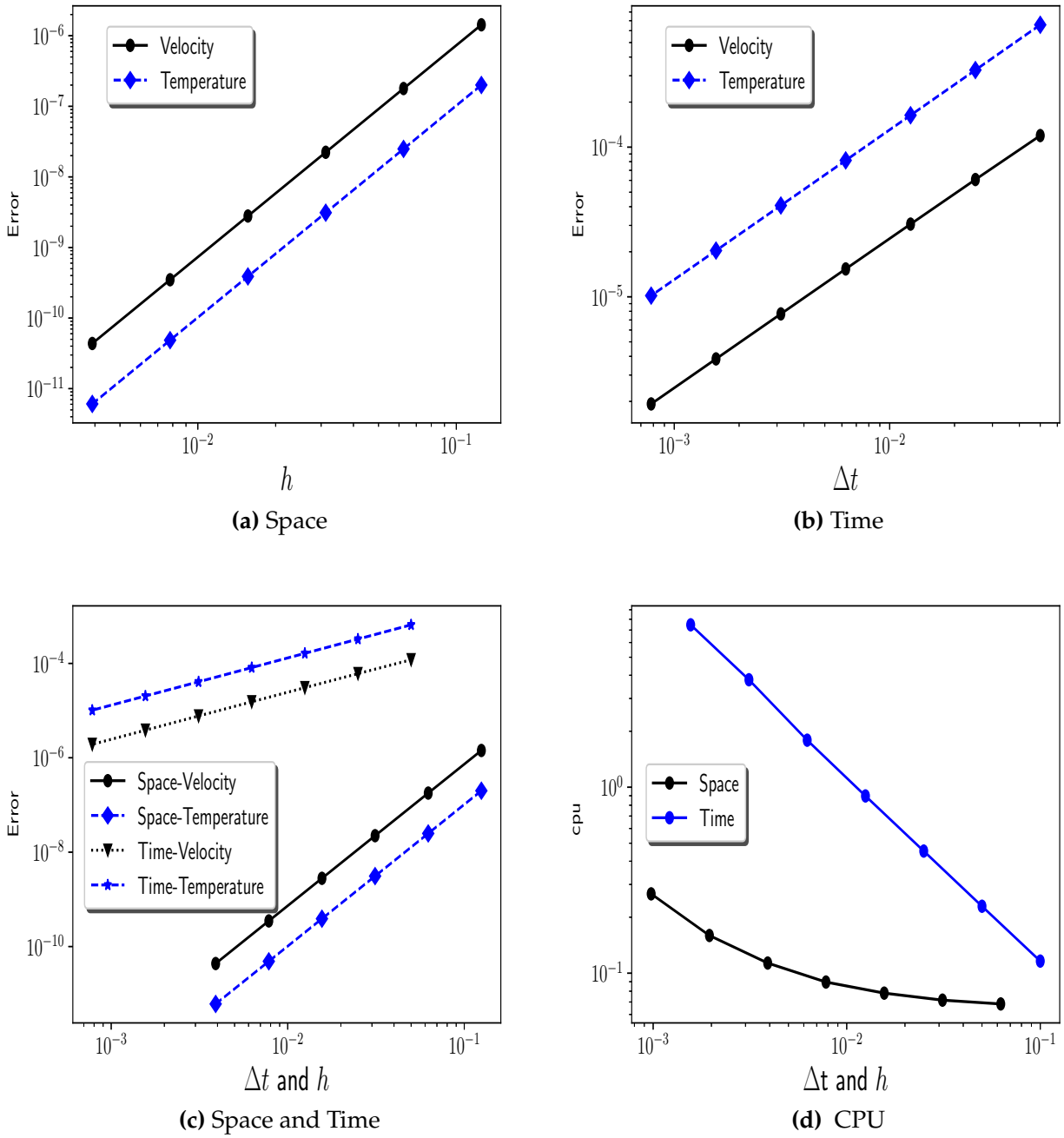

(a) Space **(b)** Time

(c) Space and Time **(d)** CPU

Figure 2. Mesh dependent convergence tests and CPU time analysis for velocity and temperature where $\gamma = 0.1$, $\mathrm{Pr} = 0.71$, $\lambda = 0.1$, $\epsilon = 0.01$, $\mathrm{Bi} = 0.1$, $T = 0.8$

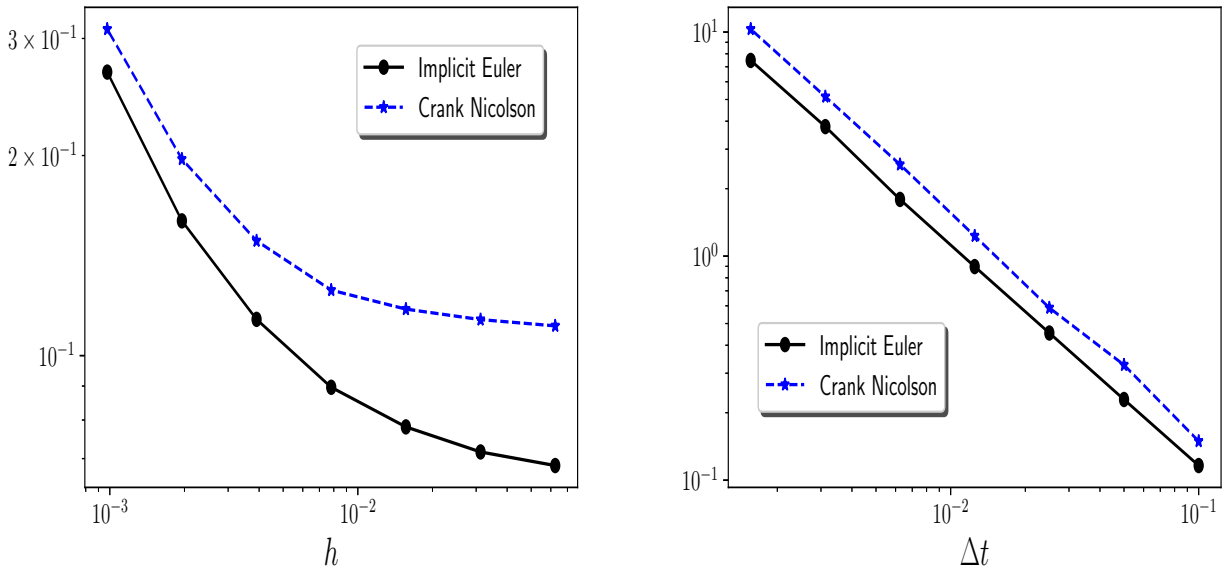

(a) Space **(b)** Time

Figure 3. CPU time comparison of Implicit Euler and Crank–Nicolson methods in time discretization for velocity where $\gamma = 0.1$, $\mathrm{Pr} = 0.71$, $\lambda = 0.1$, $\epsilon = 0.01$, $\mathrm{Bi} = 0.1$, $T = 0.8$

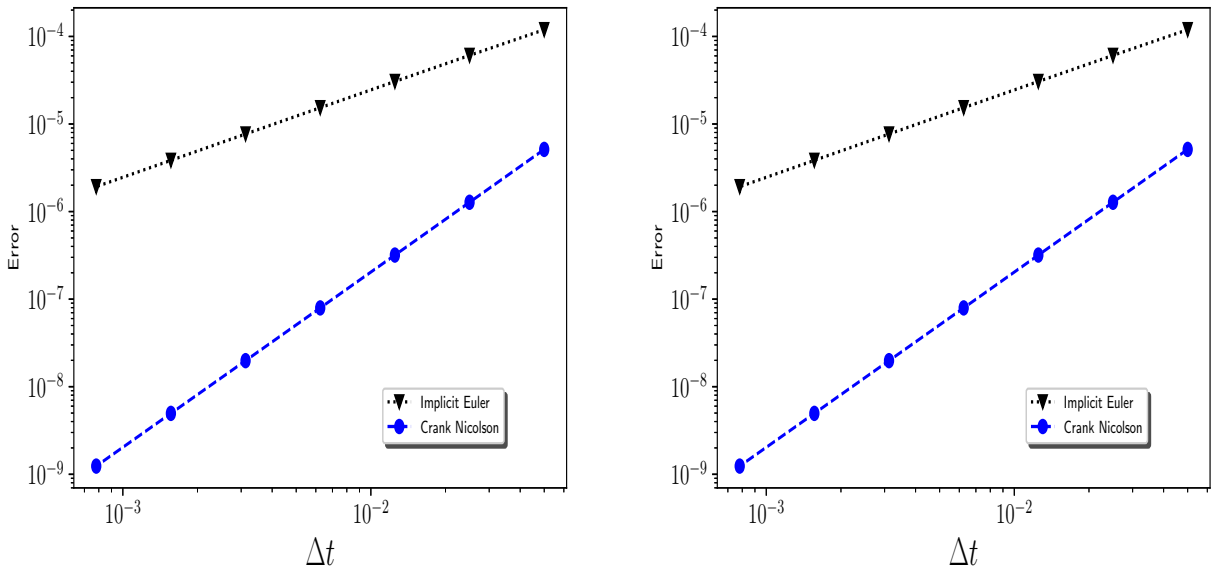

(a) Velocity **(b)** Temperature

Figure 4. Mesh dependent convergence comparison of Implicit Euler and Crank–Nicolson methods in time discretization where $\gamma = 0.1$, $\mathrm{Pr} = 0.71$, $\lambda = 0.1$, $\epsilon = 0.01$, $\mathrm{Bi} = 0.1$, $T = 0.8$

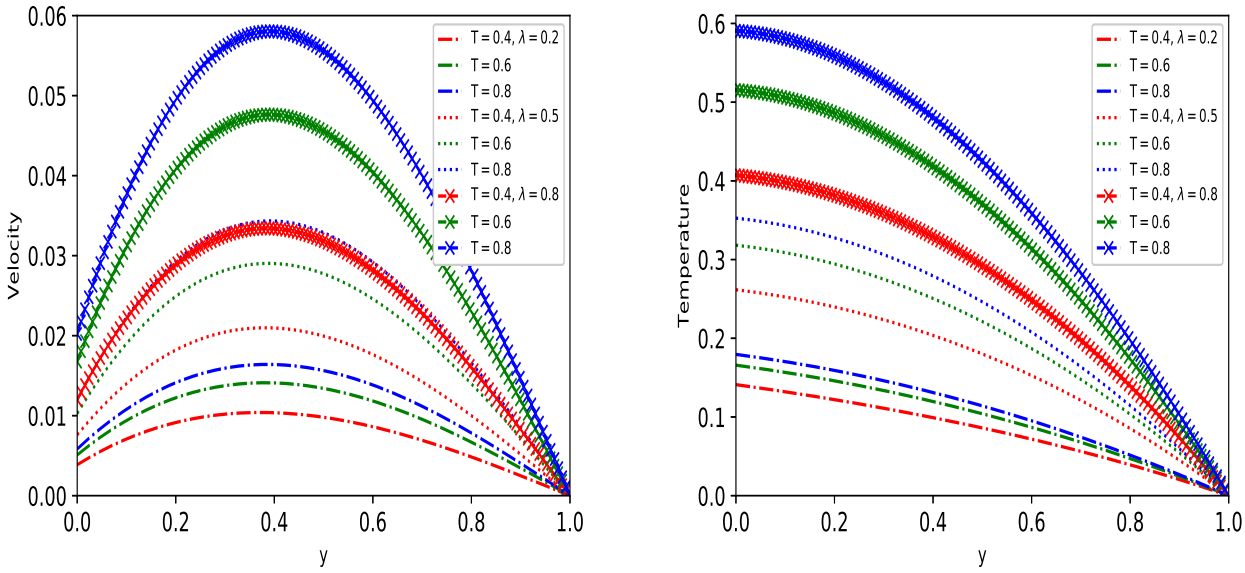

(a) Velocity **(b)** Temperature

Figure 5. Velocity and temperature profiles for several values of λ and final time T

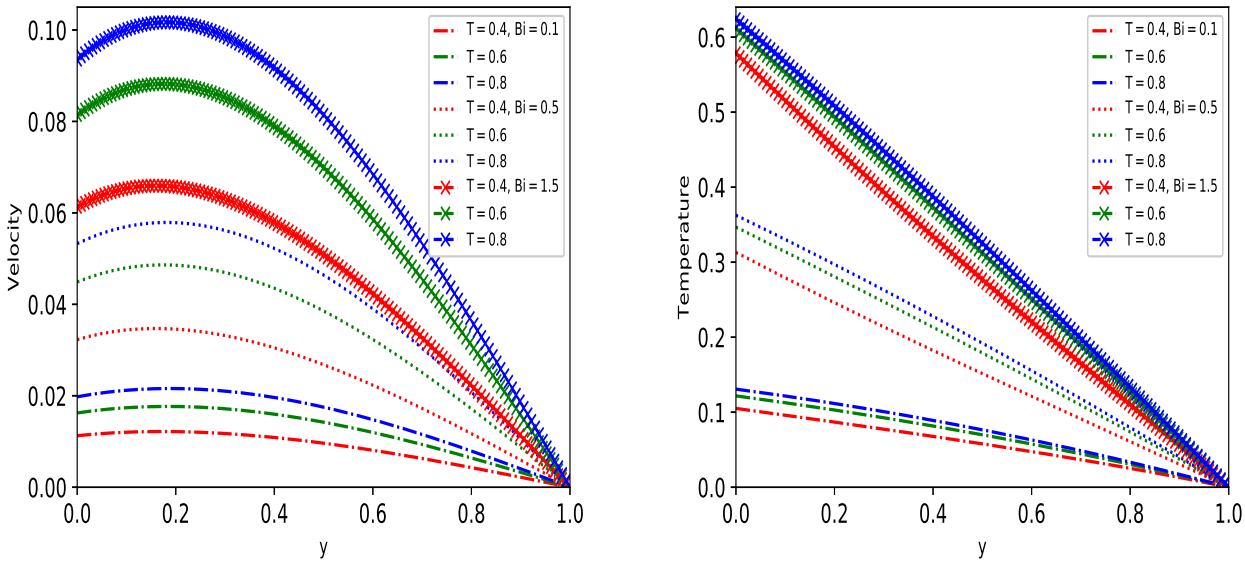

(a) Velocity **(b)** Temperature

Figure 6. Velocity and temperature profiles for several values of Bi and final time T

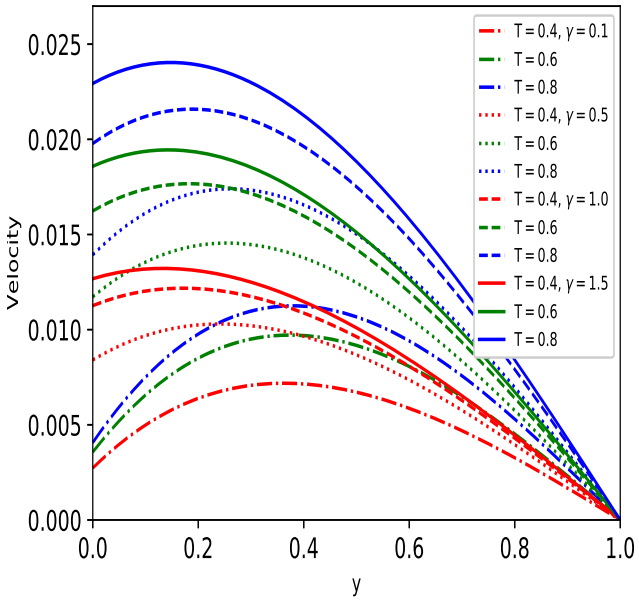

Figure 7. Velocity profiles for several values of γ and final time T

Table 1. Velocity and Temperature values for several values of ϵ when Bi $= 0.1$, Pr $= 0.71$, $\lambda = 0.1$, $\gamma = 0.1$, $T = 0.8$ and $dt = 0.1$

ϵ	$u_{\max}$	$\theta_{\max}$
1.0	$1.12234204 \times 10^{-2}$	$1.30376904 \times 10^{-}1$
10^{-1}	$1.12492495 \times 10^{-2}$	$1.30680323 \times 10^{-}1$
10^{-2}	$1.12520966 \times 10^{-2}$	$1.30714049 \times 10^{-}1$
10^{-3}	$1.12523843 \times 10^{-2}$	$1.30717459 \times 10^{-}1$
10^{-4}	$1.12524131 \times 10^{-2}$	$1.30717801 \times 10^{-}1$
10^{-5}	$1.12524160 \times 10^{-2}$	$1.30717835 \times 10^{-}1$
10^{-6}	$1.12524163 \times 10^{-2}$	$1.30717838 \times 10^{-}1$

velocity, since an increase of γ leads to an increase in the reaction and slipperiness of the lower plate surface.

On the other hand, the effects of the Frank Kamenetskii parameter (λ) are studied on the boundaries in terms of the skin friction and the Nusselt number. According to Figure 8a and Figure 8b, the wall shear stress increases as λ and t increase at both lower and upper plates. However, an increment in λ decreases the rate of heat transfer, the Nusselt number, at the lower plate, while it causes an increment at the upper plate, as shown in Figure 9a and Figure 9b.

Moreover, the observations on the skin friction and the Nusselt number are also obtained with respect to the Biot number (Bi). Increasing Bi and time t increase the skin friction on both lower and upper plates in Figure 10a and Figure 10b. Although the trend is similar for the Nusselt number at the upper plate, an increase in time causes a reverse effect on the lower plate, as shown in Figure 11a and Figure 11b. Lastly, the behavior of the skin friction is investigated with respect to the Navier slip parameter as well. Figure 12a and Figure 12b demonstrate that the wall shear stress decreases at the lower plate but it increases on the upper plate as γ increases.

Having ensured that the simulation results obtained via FEM imply that they are consistent with the results given by Hamza [26], optimal control solutions are presented in the next section.

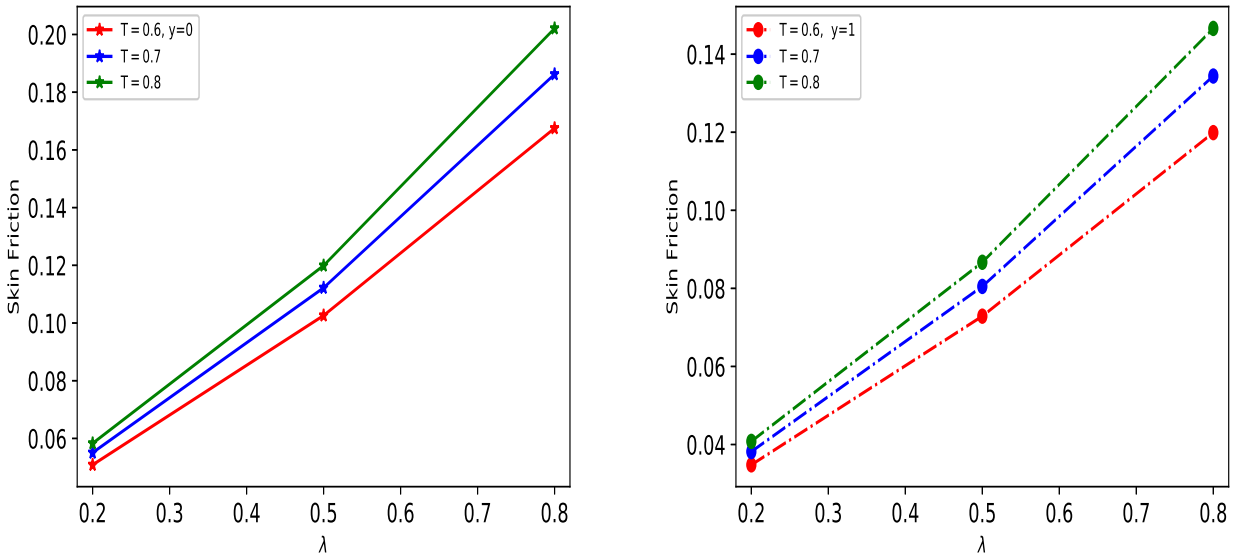

(a) $y = 0$ **(b)** $y = 1$

Figure 8. Skin friction against λ

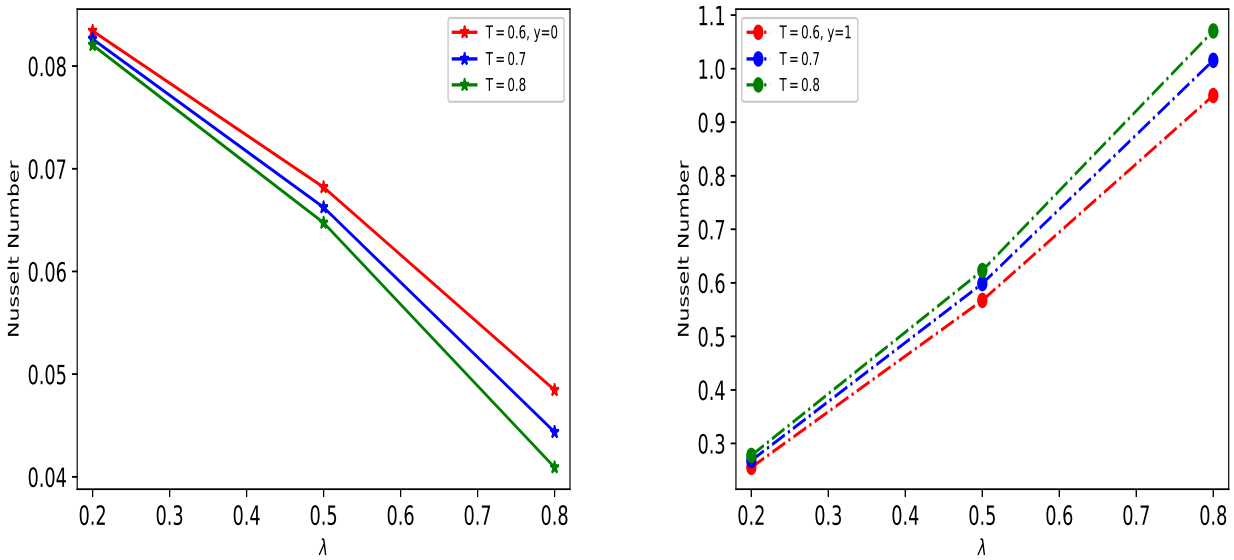

(a) $y = 0$ **(b)** $y = 1$

Figure 9. Nusselt number against λ

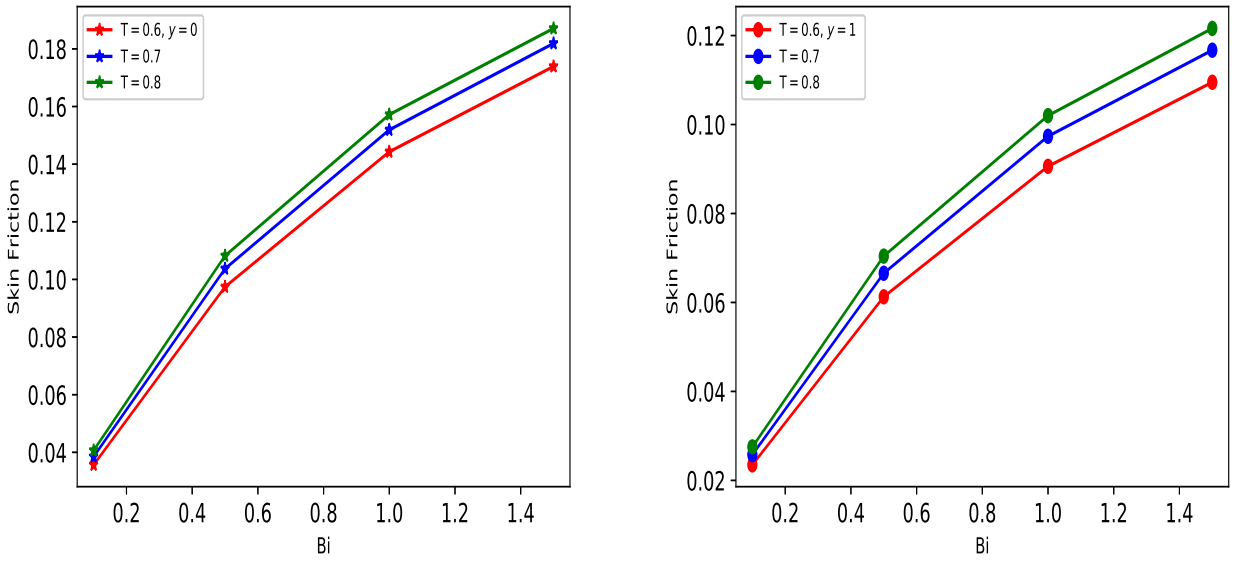

(a) $y = 0$ **(b)** $y = 1$

Figure 10. Skin friction against Bi

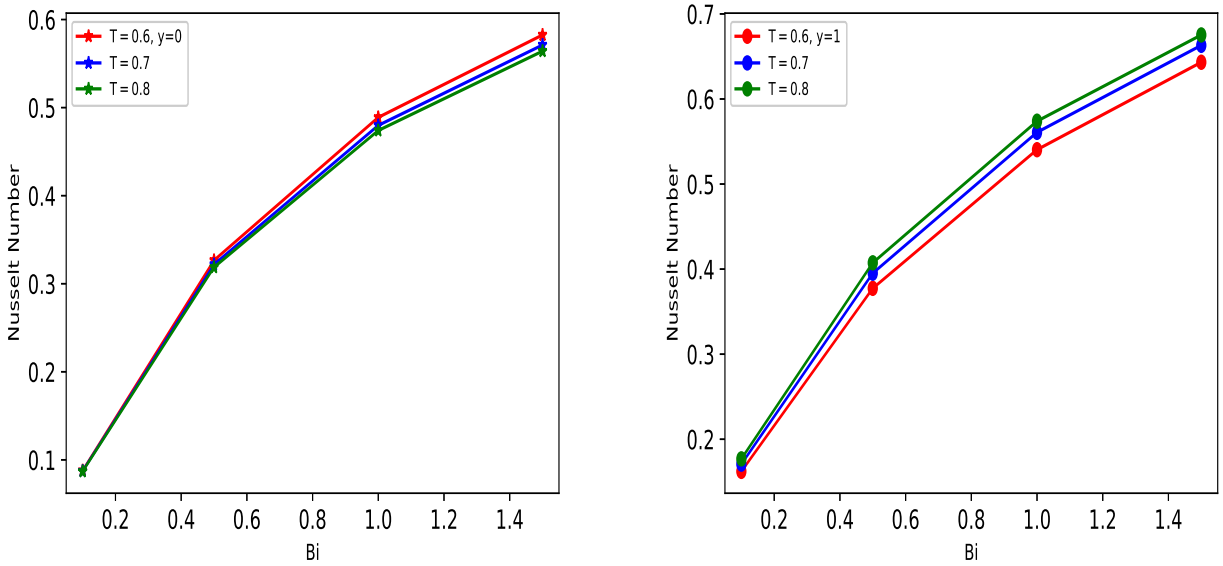

(a) $y = 0$ **(b)** $y = 1$

Figure 11. Nusselt number against Bi

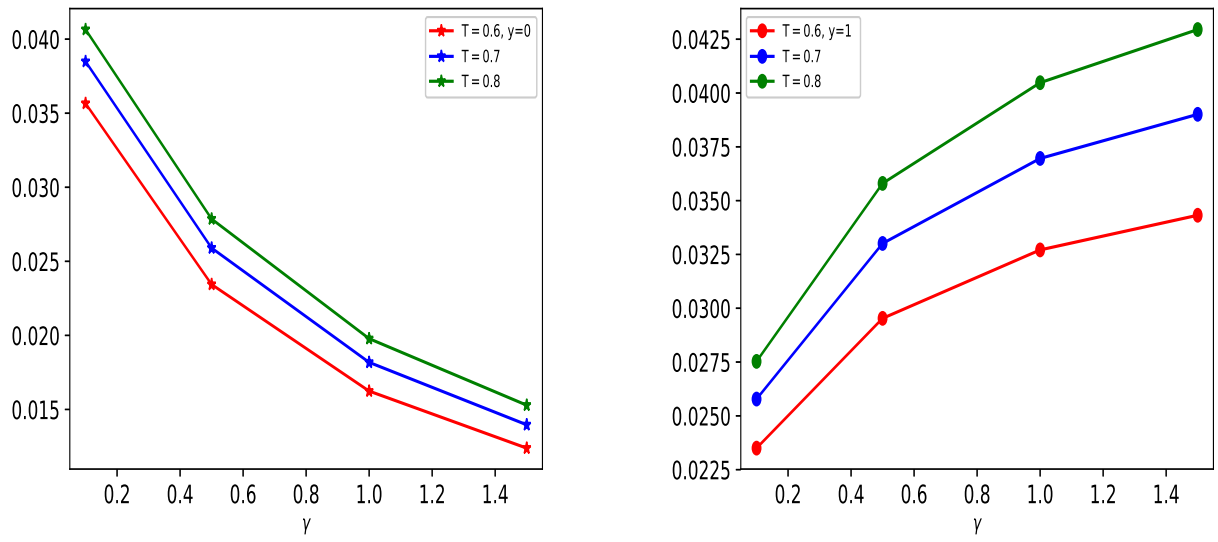

(a) $y = 0$ **(b)** $y = 1$

Figure 12. Skin friction against γ

Control simulations via FEM solutions

Having shown the dynamics of the system according to the significant parameters, the exothermic fluid flow with heat transfer is examined as an optimal control problem by controlling the fluid velocity and temperature on the lower plate. The main idea of this structure is based on the capability of driving the fluid flow into predefined or desired profiles by using the information on the boundary conditions. Hence, control formulations are taken into consideration from two perspectives: (a) control variables are chosen as the parameters in Eq. (6), which means that the slip parameter (γ) and/or the Biot number (Bi) are used to control the fluid flow and temperature on the boundary Γ_0; (b) control functions are chosen as the functions on the right-hand sides of the boundary conditions given in Eq. (6). That is, $f(t)$ and/or $g(t)$ in (11) are used to control the time-dependent velocity and/or the temperature profiles on the boundary Γ_0.

In the following, the SLSQP (Sequential Least Squares Programming) algorithm is implemented using the SciPy [32] minimization subroutine of dolfin–adjoint platform [33]. Iterations to find optimal solutions are continued until the norm of the gradient of the reduced cost function becomes less than the value of tolerance 10^{-7}. The value of each regularization parameter is reported in the corresponding caption of the related table.

It is well-known that the Navier slip parameter is used to describe the behaviour of a fluid in contact with a solid surface, and it dominates the slipperiness of the fluid along the boundary. Therefore, the first trial in the parameter control is conducted by the Navier slip parameter (γ). Desired/predefined states are produced by considering several values of γ, denoted by γ^d, and resulting optimal values, denoted by γ^{opt}, are given in Table 2. Simulation results confirm the convergence of optimal solutions and show the larger the values of γ the larger the number of iterations.

Another significant parameter of the system is the Biot number as it helps design an efficient cooling system or reaction conditions by providing information about the heat transfer characteristic of the fluid. Hence, second trial in parameter control is handled with the Biot number (Bi). To exemplify both cases - uniform and non-uniform temperature distribution within the body- desired states are generated for Biot number values that are less than and greater than 1. As

Table 2. Boundary control on the velocity with γ when Bi $= 0.1$, Pr $= 0.71$, $\lambda = 0.1$, dt $= 0.1$, $\alpha_u = \alpha_\theta = 10^3$, $\alpha_c = 10^{-5}$ and $\alpha_f = \alpha_g = 0$

γ^d	γ^{opt}	T	$\|u^{\text{opt}} - u^d\|$	$\|\theta^{\text{opt}} - \theta^d\|$	$\|\nabla \tilde{J}\|$	Nit
0.1	0.099993	0.4	7.7768×10^{-8}	1.5268×10^{-15}	6.6726×10^{-12}	8
0.1	0.099997	0.6	5.7349×10^{-8}	2.1666×10^{-15}	6.4115×10^{-10}	7
0.1	0.099998	0.8	3.8418×10^{-8}	2.6305×10^{-15}	1.3758×10^{-12}	7
0.5	0.49974	0.4	1.0914×10^{-6}	1.5268×10^{-15}	1.9446×10^{-10}	11
0.5	0.49991	0.6	6.2944×10^{-7}	2.1666×10^{-15}	2.9803×10^{-10}	10
0.5	0.49995	0.8	4.4587×10^{-7}	2.6305×10^{-15}	1.1840×10^{-9}	9
1.0	0.99723	0.4	4.9915×10^{-6}	1.5268×10^{-15}	5.8785×10^{-10}	13
1.0	0.99913	0.6	2.7322×10^{-6}	2.1666×10^{-15}	2.5992×10^{-10}	12
1.0	0.99957	0.8	1.8571×10^{-6}	2.6305×10^{-15}	3.7800×10^{-10}	11
1.5	1.48683	0.4	1.3283×10^{-5}	1.5268×10^{-15}	4.9451×10^{-12}	15
1.5	1.49603	0.6	7.1579×10^{-5}	2.1666×10^{-15}	7.3509×10^{-13}	14
1.5	1.49813	0.8	4.7749×10^{-6}	2.6305×10^{-15}	5.2228×10^{-13}	13

Table 3. Boundary control on the temperature with Bi when $\gamma = 1.0$, Pr $= 0.71$, $\lambda = 0.1$, dt $= 0.1$, $\alpha_u = \alpha_\theta = 10^3$, $\alpha_c = 10^{-5}$ and $\alpha_f = \alpha_g = 0$

Bi^d	Bi$^{\text{opt}}$	T	$\|u^{\text{opt}} - u^d\|$	$\|\theta^{\text{opt}} - \theta^d\|$	$\|\nabla \tilde{J}\|$	Nit
0.1	0.099999	0.4	3.2628×10^{-10}	2.2907×10^{-9}	1.3073×10^{-8}	6
0.1	0.099999	0.6	3.1486×10^{-10}	1.7851×10^{-9}	1.4673×10^{-9}	6
0.1	0.099999	0.8	2.9755×10^{-10}	1.4915×10^{-9}	1.9754×10^{-12}	7
0.5	0.49999	0.4	2.6455×10^{-9}	1.7730×10^{-8}	2.9641×10^{-12}	10
0.5	0.49999	0.6	2.6720×10^{-9}	1.4374×10^{-8}	7.0737×10^{-10}	9
0.5	0.49999	0.8	2.5839×10^{-9}	1.2340×10^{-8}	3.9534×10^{-9}	9
1.5	1.49999	0.4	1.9357×10^{-8}	1.1921×10^{-7}	5.3230×10^{-13}	11
1.5	1.49999	0.6	2.0812×10^{-8}	1.0280×10^{-7}	2.1376×10^{-8}	10
1.5	1.49999	0.8	2.0355×10^{-8}	9.0851×10^{-8}	2.8199×10^{-8}	9

indicated in Table 3, optimal solutions successfully reach the desired outcomes with a relatively small number of iterations compared to the control of γ.

Considering their significant effects on the physics of the problem, the next trial is to consider the pairwise control of the Navier slip parameter and the Biot number. So, Table 4 summarizes the accurately attained optimal solutions to the desired states corresponding to the several values of both parameters. As expected, doubling the control parameter relatively increases the number of iterations in the optimization.

As a forward version of the control design, the time-dependence of the boundary conditions is examined. Firstly, the time-dependent control on the boundary is adapted on the velocity as $f(t)$. Although Table 2 ensures that the number of iterations is not affected by an increase in the final time, the dependence of the control function $(f(t))$ on time clearly increases it due to the increase in the number of control variables as shown in Table 5.

Secondly, the boundary condition of the temperature field is modeled as a time-dependent control. Results in Table 6 ensure that the number of iterations increases with the increase in the number of control variables. Fortunately, pairwise but time-dependent controls on both boundaries also give promising results in achieving the predefined states, albeit at the cost of an increased number of iterations as shown in Table 7.

Table 4. Boundary control on the velocity and temperature with γ and Bi when Pr $= 0.71$, $\lambda = 0.1$, dt $= 0.1$, $\alpha_u = \alpha_\theta = 10^3$, $\alpha_c = 10^{-5}$ and $\alpha_f = \alpha_g = 0$

Bi^d	$\mathrm{Bi}^{\mathrm{opt}}$	γ	γ^d	T	$\|V^{\mathrm{opt}} - V^d\|$	$\|\theta^{\mathrm{opt}} - \theta^d\|$	$\|\nabla \tilde{J}\|$	Nit
0.1	0.099993	0.1	0.1	0.4	7.7480×10^{-8}	2.9014×10^{-9}	2.6911×10^{-8}	11
0.1	0.099997	0.1	0.1	0.6	5.0183×10^{-8}	2.0860×10^{-9}	4.5499×10^{-8}	10
0.1	0.099998	0.1	0.1	0.8	3.8239×10^{-8}	1.5054×10^{-9}	3.5604×10^{-8}	10
0.5	0.49973	0.1	0.1	0.4	1.0914×10^{-6}	1.1498×10^{-7}	9.3493×10^{-8}	14
0.5	0.49990	0.1	0.1	0.6	6.2934×10^{-7}	7.7391×10^{-8}	7.2238×10^{-8}	13
0.5	0.49995	0.1	0.1	0.8	4.4600×10^{-7}	5.9179×10^{-8}	1.7253×10^{-10}	11
1.0	0.99719	0.1	0.1	0.4	4.9912×10^{-6}	6.3378×10^{-7}	5.8242×10^{-8}	17
1.0	0.999108	0.1	0.1	0.6	2.7330×10^{-6}	4.1556×10^{-7}	1.4882×10^{-8}	15
1.0	0.99956	0.1	0.1	0.8	1.8586×10^{-6}	3.0947×10^{-7}	1.6829×10^{-10}	13
1.0	0.999667	0.5	0.5	0.4	1.7187×10^{-6}	2.0760×10^{-7}	3.6031×10^{-8}	17
1.0	0.999887	0.5	0.5	0.6	9.6693×10^{-7}	1.3613×10^{-7}	1.7495×10^{-8}	16
1.0	0.999942	0.5	0.5	0.8	6.7210×10^{-7}	1.0045×10^{-7}	1.8546×10^{-9}	19
1.0	0.999863	1.0	1.0	0.4	1.1025×10^{-6}	9.2621×10^{-8}	7.9800×10^{-9}	23
1.0	0.99995	1.0	1.0	0.6	6.3447×10^{-7}	5.2555×10^{-8}	3.9420×10^{-9}	17
1.0	0.99997	1.0	1.0	0.8	4.4821×10^{-7}	3.3231×10^{-8}	2.7437×10^{-8}	18
1.0	0.999913	1.5	1.49999	0.4	8.8241×10^{-7}	5.1638×10^{-10}	3.7148×10^{-9}	18
1.0	0.999968	1.5	1.49999	0.6	5.1567×10^{-7}	2.4156×10^{-8}	1.1175×10^{-9}	19
1.0	0.999983	1.5	1.49999	0.8	3.6812×10^{-7}	3.3102×10^{-8}	1.9883×10^{-9}	16

Table 5. Time-dependent boundary control on the velocity when Bi $= 0.1$, Pr $= 0.71$, $\lambda = 0.1$, dt $= 0.1$, $\alpha_u = \alpha_\theta = 10^3$, $\alpha_f = 10^{-5}$ and $\alpha_c = \alpha_g = 0$

γ^d	T	$\|u^{\mathrm{opt}} - u^d\|$	$\|\nabla \tilde{J}\|$	Nit
0.1	0.4	2.5224×10^{-18}	1.9183×10^{-9}	8
0.1	0.6	9.6826×10^{-18}	1.9035×10^{-9}	10
0.1	0.8	2.0998×10^{-17}	1.1211×10^{-8}	12
0.5	0.4	3.5764×10^{-18}	4.8549×10^{-10}	8
0.5	0.6	1.4501×10^{-17}	1.6843×10^{-9}	10
0.5	0.8	8.4691×10^{-18}	5.3934×10^{-9}	12
1.0	0.4	2.1804×10^{-18}	1.3929×10^{-8}	7
1.0	0.6	4.7359×10^{-18}	1.2594×10^{-9}	10
1.0	0.8	1.1069×10^{-17}	3.0075×10^{-9}	12

Table 6. Time-dependent boundary control on the temperature when $\gamma = 1.0$, Pr $= 0.71$, $\lambda = 0.1$, dt $= 0.1$, $\alpha_u = \alpha_\theta = 10^3$, $\alpha_g = 10^{-5}$ and $\alpha_c = \alpha_f = 0$

Bi^d	T	$\|u^{\mathrm{opt}} - u^d\|$	$\|\theta^{\mathrm{opt}} - \theta^d\|$	$\|\nabla \tilde{J}\|$	Nit
0.1	0.4	7.5911×10^{-16}	3.3008×10^{-15}	8.7364×10^{-10}	10
0.1	0.6	6.4731×10^{-16}	1.9490×10^{-15}	5.1838×10^{-9}	13
0.1	0.8	4.7463×10^{-16}	1.1373×10^{-15}	1.1200×10^{-8}	12
0.5	0.4	3.5092×10^{-13}	1.4730×10^{-12}	1.0127×10^{-8}	9
0.5	0.6	2.9075×10^{-13}	8.3834×10^{-13}	6.1592×10^{-10}	10
0.5	0.8	2.1094×10^{-13}	4.7483×10^{-13}	1.0850×10^{-8}	13
1.5	0.4	1.8122×10^{-11}	7.3563×10^{-11}	5.9525×10^{-12}	7
1.5	0.6	1.4818×10^{-11}	4.1874×10^{-11}	1.4847×10^{-9}	11
1.5	0.8	1.0694×10^{-11}	2.3830×10^{-11}	1.1199×10^{-9}	13

Table 7. Time-dependent boundary control on the velocity and temperature when Pr $= 0.71$, $\lambda = 0.1$, dt $= 0.1$, $\alpha_u = \alpha_\theta = 10^3$, $\alpha_f = \alpha_g = 10^{-5}$ and $\alpha_c = 0$

γ^d	Bi^d	T	$\|u^{\mathrm{opt}} - u^d\|$	$\|\theta^{\mathrm{opt}} - \theta^d\|$	$\|\nabla \tilde{J}\|$	Nit
0.1	0.1	0.4	1.0221×10^{-15}	3.3008×10^{-15}	3.0714×10^{-9}	14
0.1	0.1	0.6	9.6972×10^{-16}	1.9490×10^{-15}	2.0665×10^{-9}	16
0.1	0.1	0.8	7.9573×10^{-16}	1.1373×10^{-15}	3.6916×10^{-9}	18
0.5	0.1	0.4	1.0241×10^{-15}	3.3008×10^{-15}	4.3539×10^{-9}	14
0.5	0.1	0.6	9.9628×10^{-16}	1.9490×10^{-15}	1.8661×10^{-9}	16
0.5	0.1	0.8	8.1904×10^{-16}	1.1373×10^{-15}	2.5095×10^{-9}	18
1.5	0.1	0.4	1.0310×10^{-15}	3.3008×10^{-15}	4.9799×10^{-9}	14
1.5	0.1	0.6	9.8253×10^{-16}	1.9490×10^{-15}	9.9845×10^{-9}	15
1.5	0.1	0.8	8.2242×10^{-16}	1.1373×10^{-15}	1.1631×10^{-8}	17
1.0	0.5	0.4	4.7809×10^{-13}	1.4730×10^{-12}	1.3276×10^{-8}	11
1.0	0.5	0.6	4.4646×10^{-13}	8.3834×10^{-13}	1.6377×10^{-8}	14
1.0	0.5	0.8	3.6590×10^{-13}	4.7483×10^{-13}	5.8150×10^{-9}	17
1.0	1.0	0.4	6.3718×10^{-12}	1.9152×10^{-11}	2.8537×10^{-10}	12
1.0	1.0	0.6	5.9025×10^{-11}	1.0892×10^{-11}	1.0109×10^{-8}	15
1.0	1.0	0.8	4.8214×10^{-12}	6.1845×10^{-12}	6.1752×10^{-9}	17
1.0	1.5	0.4	2.4821×10^{-11}	7.3563×10^{-11}	2.4928×10^{-9}	14
1.0	1.5	0.6	2.2899×10^{-11}	4.1874×10^{-11}	1.1292×10^{-8}	18
1.0	1.5	0.8	1.8676×10^{-11}	2.3830×10^{-11}	2.8764×10^{-9}	21

5 Conclusion

The unsteady free convective flow of reactive viscous fluid is studied with heat transfer within an exothermic reaction under Arrhenius kinetics and the Navier slip condition on the lower surface of the vertical channel. In the present paper, the Navier slip parameter and Biot number are designed as control parameters to derive the fluid into desired velocity and temperature. The control of the flow is also attained by the time-dependent functions of the boundary conditions of the problem. A discretize-then-optimize approach is applied with the SLSQP(Sequential Least Squares Programming) algorithm in the optimization. Direct and optimal control solutions are formulated by using quadratic finite element approximations of the PDEs. Numerical simulations of the unsteady fluid flow equations are obtained with several values of the parameters to demonstrate that they accurately reflect the dynamics of the problem. Therefore, the findings of this study provide reliable approximate direct solutions via FEM and contribute to optimal control strategies on the boundary for an exothermic fluid flow with Navier slip condition. As a future work of this study, it is possible to expand the problem domain into a 2D or 3D framework.

Declarations

Use of AI tools

The author declares that she has not used Artificial Intelligence (AI) tools in the creation of this article.

Data availability statement

No Data associated with the manuscript.

Ethical approval (optional)

The author declares that this research complies with ethical standards. This research does not involve human participants or animals.

Consent for publication

Not applicable

Conflicts of interest

The author declares that she has no conflict of interest.

Funding

No funding was received for this research.

Author's contributions

The author has read and agreed to the published version of the manuscript.

Acknowledgements

Not applicable

References

[1] Minto, B.J. and Ingham, D.B. and Pop, I. Free convection driven by an exothermic reaction on a vertical surface embedded in porous media. *International Journal of Heat and Mass Transfer,* 41(1), 11-23, (1998). [CrossRef]

[2] Makinde, O.D. Thermal stability of a reactive viscous flow through a porous-saturated channel with convective boundary conditions. *Applied Thermal Engineering*, 29(8-9), 1773-1777, (2009). [CrossRef]

[3] Jha, B.K. and Samaila, A.K. and Ajibade, A.O. Transient free-convective flow of reactive viscous fluid in a vertical channel. *International Communications in Heat and Mass Transfer,* 38(5), 633-637, (2011). [CrossRef]

[4] Jha, B. K. and Samaila, A. K. and Ajibade, A. O. Transient free-convective flow of reactive viscous fluid in vertical tube. *Mathematical and Computer Modelling*, 54(11-12), 2880-2888, (2011). [CrossRef]

[5] Bhat, I.A. and Mishra, L.N. A comparative study of discretization techniques for augmented Urysohn type nonlinear functional Volterra integral equations and their convergence analysis. *Applied Mathematics and Computation*, 470, 128555, (2024). [CrossRef]

[6] Bhat, I.A., Mishra, L.N., Mishra, V.N., Abdel-Aty, M. and Qasymeh, M. A comprehensive analysis for weakly singular nonlinear functional Volterra integral equations using discretization techniques. *Alexandria Engineering Journal*, 104, 564-575, (2024). [CrossRef]

[7] Rao, I.J. and Rajagopal, K.R. The effect of the slip boundary condition on the flow of fluids in a channel. *Acta Mechanica*, 135, 113-126, (1999). [CrossRef]

[8] Rundora, L. and Makinde, O.D. Effects of Navier slip on unsteady flow of a reactive variable viscosity non-Newtonian fluid through a porous saturated medium with asymmetric convective boundary conditions. *Journal of Hydrodynamics*, 27, 934-944, (2015). [CrossRef]

[9] Gbadeyan, J.A. and Abubakar, J.U. and Oyekunle, T.L. Effects of Navier slip on a steady flow of an incompressible viscous fluid confined within spirally enhanced channel. *Journal of the Egyptian Mathematical Society*, 28, 32, (2020). [CrossRef]

[10] Tauviqirrahman, M. and Ismail, R. and Schipper, D.J. Optimization of the complex slip

surface and its effect on the hydrodynamic performance of two-dimensional lubricated contacts. *Computers & Fluids*, 79, 27-43, (2013). [CrossRef]

[11] Zhang, H., Liu, Y., Dai, S., Li, F. and Dong, G. Optimization of boundary slip region on bearing sliders to improve tribological performance. *Tribology International*, 168, 107446, (2022). [CrossRef]

[12] Hu, W. and Wu, J. An approximating approach for boundary control of optimal mixing via Navier-Stokes flows. *Journal of Differential Equations*, 267(10), 5809-5850, (2019). [CrossRef]

[13] Haslinger, J. and Mäkinen, R.A. The parameter identification in the Stokes system with threshold slip boundary conditions. *Journal of Applied Mathematics and Mechanics/Zeitschrift für Angewandte Mathematik und Mechanik*, 100(5), e201900209, (2020). [CrossRef]

[14] Zhang, W. and Zhu, B. Optimization design for slip/no-slip configuration of hydrophobic sliding bearings using Monte Carlo search. *Tribology International*, 178, 108034, (2023). [CrossRef]

[15] Kunisch, K. and Marduel, X. Optimal control of non-isothermal viscoelastic fluid flow. *Journal of Non-Newtonian Fluid Mechanics*, 88(3), 261-301, (2000). [CrossRef]

[16] Gunzburger, M.D. and Manservisi, S. The velocity tracking problem for Navier–Stokes flows with boundary control. *SIAM Journal on Control and Optimization*, 39(2), 594-634, (2000). [CrossRef]

[17] Lee, H.C. and Imanuvilov, O.Y. Analysis of Neumann boundary optimal control problems for the stationary Boussinesq equations including solid media. *SIAM Journal on Control and Optimization*, 39(2), 457-477, (2000). [CrossRef]

[18] Mallea-Zepeda, E. and Lenes, E. and Valero, E. Boundary control problem for heat convection equations with slip boundary condition. *Mathematical Problems in Engineering*, 2018(1), 7959761, (2018). [CrossRef]

[19] Thalakkottor, J.J. and Mohseni, K. Unified slip boundary condition for fluid flows. *Physical Review E*, 94(2), 023113, (2016). [CrossRef]

[20] Málek, J. and Rajagopal, K.R. On determining Navier's slip parameter at a solid boundary in flows of a Navier–Stokes fluid. *Physics of Fluids*, 36(1), (2024). [CrossRef]

[21] Evcin, C. and Uğur, Ö. and Tezer-Sezgin, M. Determining the optimal parameters for the MHD flow and heat transfer with variable viscosity and Hall effect. *Computers & Mathematics with Applications*, 76(6), 1338-1355, (2018). [CrossRef]

[22] Evcin, C. and Uğur, Ö. and Tezer-Sezgin, M. Controlling the power-law fluid flow and heat transfer under the external magnetic field using the flow index and the Hartmann number. *International Journal of Computational Methods*, 17(03), 1850143, (2020). [CrossRef]

[23] Evcin, C. and Uğur, Ö. and Tezer-Sezgin, M. Time varying control of magnetohydrodynamic duct flow. *European Journal of Mechanics-B/Fluids*, 89, 100-114, (2021). [CrossRef]

[24] Evcin, C. and Uğur, Ö. and Tezer-Sezgin, M. Optimal placement of the multiple magnetic sources for the MHD flow in a rectangular duct. *Optimization and Engineering*, 24, 2855-2885, (2023). [CrossRef]

[25] Bergman, T.L., Lavine, A.S., Incropera, F.P. and Dewitt, D. P. *Fundamentals of Heat and Mass Transfer.* John Wiley & Sons Hoboken: USA, (2011).

[26] Hamza, M.M. Free convection slip flow of an exothermic fluid in a convectively heated vertical channel. *Ain Shams Engineering Journal*, 9(4), 1313-1323, (2018). [CrossRef]

[27] Nocedal, J. and Wright, S.J. *Numerical Optimization*. Springer Science+Business Media: New York, (2006).

[28] Kraft, D. A software package for sequential quadratic programming. *Forschungsbericht-Deutsche Forschungs- und Versuchsanstalt fur Luft- und Raumfahrt*, (1988).

[29] Kraft, D. Algorithm 733: TOMP-Fortran modules for optimal control calculations. *ACM Transactions on Mathematical Software*, 20(3), 262-281, (1994). [CrossRef]

[30] Schittkowski, K. The nonlinear programming method of Wilson, Han, and Powell with an augmented Lagrangian type line search function Part I. *Numerische Mathematik*, 38, 83-114, (1982). [CrossRef]

[31] Logg, A., Mardal, K.A. and Wells, G. *Automated Solution of Differential Equations by the Finite Element Method* (Vol. 84). Springer- Verlag: Berlin, (2012). [CrossRef]

[32] Virtanen, P., Gommers, R., Oliphant, T.E., Haberland, M., Reddy, T., Cournapeau, D. et al. SciPy 1.0: fundamental algorithms for scientific computing in Python. *Nature Methods*, 17(3), 261-272, (2020). [CrossRef]

[33] Farrell, P.E., Ham, D.A., Funke, S.W. and Rognes, M.E. Automated derivation of the adjoint of high-level transient finite element programs. *SIAM Journal on Scientific Computing*, 35(4), c369-c393, (2013). [CrossRef]

Mathematical Modelling and Numerical Simulation with Applications (MMNSA)
(https://dergipark.org.tr/en/pub/mmnsa)

How to cite this article: Evcin, C. (2024). Boundary control of unsteady natural convective slip flow in reactive viscous fluids. *Mathematical Modelling and Numerical Simulation with Applications*, 4(5), 116-138. https://doi.org/10.53391/mmnsa.1555392